Radiation induces turbulence in particle-laden fluids

Rémi Zamansky,[1,a)] Filippo Coletti,[2,b)] Marc Massot,[1,3] and Ali Mani[1,2]
[1]*Centre for Turbulence Research, Stanford University, Stanford, California 94305-3035, USA*
[2]*Mechanical Engineering, Stanford University, California 94305-3035, USA*
[3]*Ecole Centrale Paris, Laboratoire EM2C - UPR CNRS 288 et Fédération de Mathématiques - FR CNRS 3487, Grande Voie des Vignes, 92295 Chatenay-Malabry Cedex, France*

When a transparent fluid laden with solid particles is subject to radiative heating, non-uniformities in particle distribution result in local fluid temperature fluctuations. Under the influence of gravity, buoyancy induces vortical fluid motion which can lead to strong preferential concentration, enhancing the local heating and more non-uniformities in particle distribution. By employing direct numerical simulations this study shows that the described feedback loop can create and sustain turbulence. The velocity and length scale of the resulting turbulence is not known *a priori*, and is set by balance between viscous forces and buoyancy effects. When the particle response time is comparable to a viscous time scale, introduced in our analysis, the system exhibits intense fluctuations of turbulent kinetic energy and strong preferential concentration of particles.

Turbulent flows laden by heavy particles or droplets are known to exhibit complex interactions between the continuous and the dispersed phase, notably particle preferential concentration and fluid turbulence modification.[1] In several natural phenomena, turbulent dispersed multiphase flows occur in presence of thermal radiation. In cloud physics, preferential concentration is believed to play an important role in determining the rate of droplet coalescence.[2] In circumstellar disks, turbulent clustering appears to be critical for the aggregation of chondrules and other constituents into primitive planetesimals.[3] Example in industrial applications include the injection of fuel sprays in combustion chambers,[4] particle-based solar receivers,[5] and aluminum particles in solid rocket motors.[6] However, the three-way coupled interactions between the transport modes associated with fluid flow, particles, and radiation, and their resulting radiation-induced turbulence, is not yet explored in the literature. In most previous studies, turbulence is enforced either by the inertia of the imposed flow velocity, or by a prescribed turbulent spectrum, and the effect of the radiation on the fluid motion is discarded.[7,8] In rare previous studies that account for turbulence-radiation interaction, the coupling is due to the nonlinear dependence between temperature and composition fluctuations, which is important in high temperature reactive flows.[9]

In this letter we present a system in which the incident radiative flux is the only energy input and show that it can self-sustain turbulence. Specifically, we consider a large number of randomly distributed particles immersed in a transparent fluid, and subject to thermal radiation, as shown in Fig. 1(a). We focus on the case in which the fluid is initially at rest and the particles have zero settling velocity. Non-uniformities of the gas/particle mixture result in inhomogeneities in heat absorption and therefore in spatial temperature variations. Fluid motion is induced by local gas expansion and buoyancy. The resulting baroclinic vorticity production induces higher non-uniformities by centrifuging the inertial particles leading to new non-uniformities in heat absorption. This feedback loop between local particle concentration, temperature fluctuations, and hydrodynamic forcing is schematically illustrated in Fig. 1. In this letter we show that this feedback loop can trigger and

[a)]Present address: Université de Toulouse, INPT, UPS, IMFT (Institut de Mécanique des Fluides de Toulouse), Allée Camille Soula, 31400 Toulouse, France.
[b)]Present address: University of Minnesota, Aerospace Engineering and Mechanics, 110 Union St., SE Minneapolis, Minnesota 55455, USA.

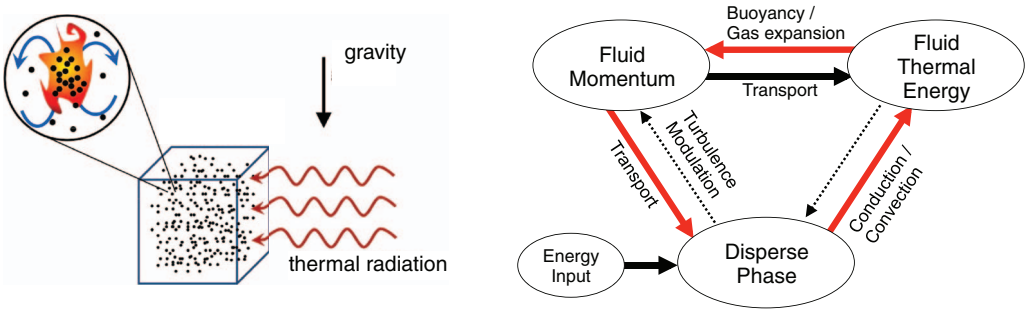

FIG. 1. (Left) Schematics of particle-laden flow subject to radiation. Buoyant plumes are induced in regions with higher particle concentration. (Right) A diagram showing the interplay between fluid momentum, fluid temperature, and particles. The plain arrows represent the leading order interactions whereas the dashed arrows represent the interactions of secondary importance. The red arrows emphasize the feedback loop.

maintain turbulence, and that the process is spontaneous and self-sustained in a large portion of the parameter space.

In order to retain the minimal physics for capturing the dynamics depicted by the cartoon of Fig. 1, the following assumptions are considered. We consider a periodic cubic domain subject to constant and homogeneous thermal radiation. The carrier phase is a gas transparent to radiation, whereas the incident radiative flux on each particle is completely absorbed. The particles are small monodisperse spheres of negligible heat capacity, and their number density is low enough to neglect mutual interactions, and to consider the fluid/particle medium as optically thin. We focus on the low radiative flux regime: in this limit, the fluid density variation is small relative to its absolute value, and is retained only in the buoyancy forcing term via the Boussinesq approximation. For the same reason, the spatial mean temperature of the system is considered as quasi-stationary over times relevant for the dynamics. Particles are assumed in thermal equilibrium with their adjacent fluid, owing to their vanishingly small heat capacity.[10] Under these assumptions the main parameters of the system are: the fluid viscosity ν, the fluid density ρ_f, the fluid specific heat capacity c_f, the fluid thermal diffusivity κ, the fluid thermal expansion coefficient α, the particle diameter d_p, the particle density ρ_p, the particle mean concentration (number density) $\overline{n}$, the radiative heat flux density Φ, the gravitational acceleration g, and the periodicity of the spatial domain H.

The aforementioned assumptions allow to model the radiative heat flux received by each particle as $\Phi_p = \frac{\pi}{4} d_p^2 \Phi$. The temperature of the system rises at a rate:

$$\beta = \frac{d\langle T \rangle_s}{dt} = \frac{\overline{n}\Phi_p}{\rho_f c_f}, \tag{1}$$

where T is the fluid temperature and $\langle \bullet \rangle_s$ indicates spatial averaging. Although highly simplified, this modeling of the radiative heating is consistent with a low volume fraction distribution of particles with negligible thermal inertia. Equation (1) implies a linear increase of the domain temperature with time. Our interest being in the local dynamics, we focus on the local fluctuations around $\langle T \rangle_s$.

Unlike classic turbulence forced at large scales, here the characteristic flow scales are inherently determined by the nonhomogeneity of the fluid/particles mixture. If we assume the response of the fluid to the local heating to be independent from the size of the domain, then dimensional analysis yields $t_* = (\alpha g \beta)^{-2/5} \nu^{1/5}$ for the temporal scale and $\ell_* = (\alpha g \beta)^{-1/5} \nu^{3/5}$ for the length scale. From the Brunt-Väisälä frequency,[11] the typical temperature fluctuation is written as $\theta_* = \beta t_*$. Our simulations indicate that these scales are of the order of the smallest scales in the present flow regime. A corresponding set of non-dimensional parameters is: the Stokes number $St = \tau_p / t_*$ (where $\tau_p = \rho_p d_p^2 / \rho_f 18\nu$ is the particle response time), the non-dimensional domain size $\gamma = H/\ell_*$, the Prandtl number $Pr = \nu/\kappa$, the Froude number $Fr = \sqrt{\ell_*/g t_*^2}$, and the non-dimensional particle number density $C = \overline{n}\ell_*^3$. We note that the Stokes number defined here, is different form the standard definition involving the Kolmogorov length. For this problem the Kolmogorov length is not known *a*

TABLE I. Parameters of the simulations. These simulations have been run for $St = 0:003, 0.019, 0.074, 0.35, 1.06, 7.34,$ and 29.4. For all cases, $Pr = 1$, and $Fr = \infty$. N is the size of the mesh in each direction, N_p is the number of particle.

γ	C	N	N_p	γ	C	N	N_p
83	0.035	128	2.00×10^4	48	0.19	64	2.13×10^4
83	0.19	128	1.10×10^5	83	0.19	128	1.10×10^5
83	0.35	128	2.00×10^5	190	0.19	256	1.34×10^6
83	1.82	128	1.036×10^6	330	0.19	512	6.96×10^6
83	8.77	128	5.00×10^6				

priori. The non-dimensional equations of motion simplified according to the Oberbeck-Boussinesq approximation[12] read

$$\nabla.\mathbf{u} = 0; \qquad D_t\mathbf{u} = -\nabla p + \nabla^2\mathbf{u} + \theta\mathbf{e_z}, \tag{2}$$

$$D_t\theta = \frac{1}{Pr}\nabla^2\theta + c', \tag{3}$$

where $D_t = \partial_t + \mathbf{u}.\nabla$, and $\theta = (T - \langle T\rangle_s)/\theta_*$ is the non-dimensional temperature fluctuation around the mean box temperature. In Eq. (2) we have not included the reaction of the particles on the fluid phase assuming a small particle loading. Retaining only the Stokes drag and the gravitational force, the particle equation of motion reads

$$d_t\mathbf{x}_p = \mathbf{u}_p; \qquad d_t\mathbf{u}_p = \frac{\mathbf{u} - \mathbf{u}_p}{St} - \frac{\mathbf{e_z}}{Fr^2}. \tag{4}$$

The thermal source term in Eq. (3) is associated to the fluctuations of the local particle concentration

$$c' = \sum_p^{N_p}(\delta(\mathbf{x} - \mathbf{x}_p)/C) - 1, \tag{5}$$

where $\mathbf{x}_p$ is the position of the pth particle, δ is the Dirac distribution, and N_p is the number of particles.

Equations (2) and (3) are solved using a pseudo-spectral method in a periodic cubic domain. The time integration is performed by second order Adams-Bashforth method. We use Lagrangian tracking to obtain the evolution of the particle velocities and positions. The gas velocity at the particle position is evaluated from cubic spline interpolation. The thermal source term is computed from the local particle concentration field obtained by Gaussian regularization of the Dirac masses.[13] It was checked *a posteriori* that the mesh was sufficiently fine to resolve the smallest physical scales, and that results were not affected by further grid refinement. All simulations are initiated in quiescent conditions and with particles randomly distributed in space. We perform analysis of these simulations after sufficient runtime when the statistically stationary condition is established.

We carry out simulations encompassing 7 Stokes numbers (ranging from 3×10^{-3} to 30), 4 domain sizes ($\gamma = 48$, 83, 190, and 330), and 5 mean particle concentrations ($C = 0.035$,

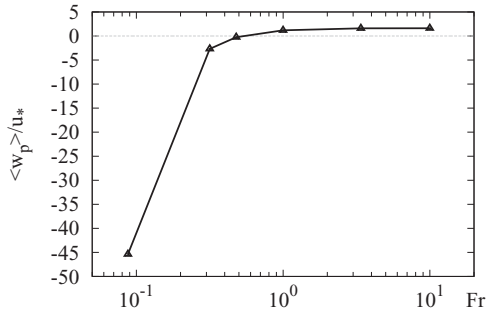

FIG. 2. Effect of the Froude number on the mean vertical velocity of particle (the settling velocity) normalized by $u_* = \ell_*/t_*$ for $St = 0.3$, $\gamma = 83$, $C = 0.35$, and $Pr = 1$.

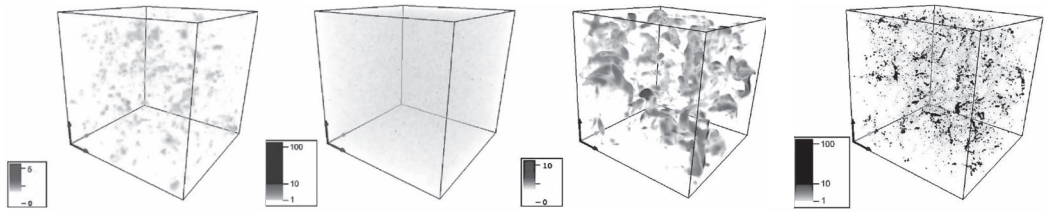

FIG. 3. Snapshots of temperature fluctuations θ/θ_* (a), and particle concentration $c' + 1$ (see Eq. (5)) (b), for $St = 0.019$. Snapshots of temperature fluctuations (note the different color map compared to (a)) (c) and particle concentration (d) for $St = 0.35$. In both cases, $\gamma = 83$, and $C = 0.35$. Images produced by VAPOR (www.vapor.ucar.edu).

0.19, 0.35, 1.82, and 8.77). For these calculations we impose $Pr = 1$, and $1/Fr = 0$ (non-settling particles). The simulation parameters are summarized in Table I. For the case $St = 0.35$, $\gamma = 83$, $C = 0.35$, and $Pr = 1$, we also explore the effect of gravitational settling by simulating 6 finite Froude numbers between 0.087 and 10. As shown in Fig. 2, the settling velocity (i.e., the negative vertical velocity) is high for $Fr < 0.32$, but negligible for Fr of order one or larger. In the latter case, both instantaneous realizations and statistics confirm that the weak gravitational settling does not affect the qualitative behavior of the system. In this paper we consider only the non-settling limit and defer the exploration of the settling effects to a future publication. In this limit the mean particle vertical velocity is slightly positive, due to the buoyancy acting on the hot fluid that surrounds them. Given this note, and assuming $Pr = 1$, the key parameters controlling the dynamics are C, γ, and St, as considered in Table I.

Fig. 3 presents snapshots of the fluid temperature and particle local concentration in the domain, for $St = 0.019$ and contrasts it to the case with $St = 0.35$. For small particle inertia the fields are fairly homogeneous, whereas at higher Stokes number plumes of high temperature appear in correspondence of highly concentrated particle clusters. The accretion and disaggregation of the clusters is entangled with the formation, merging and expansion of the hot plumes that surround them. Additionally, the St $= 0.35$ case, results in much larger fluctuations of the fluid velocity with high degree of intermittency. This is illustrated in Fig. 4, that shows the temporal evolution of the turbulent kinetic energy in the box (TKE $= 0.5\langle \mathbf{u}.\mathbf{u} \rangle_s$), for three Stokes numbers $St = 0.019$, 0.35, and 7.3. The turbulent kinetic energy is normalized by $u_* = \ell_*/t_*$, which is independent of the particle inertial relaxation time, τ_p. After an initial spin up ($t/t_* < 50$), the system reaches its statistically stationary condition. The influence of the particle response time on the dynamics is evident: at low Stokes number the system presents a relatively low level of turbulent kinetic energy and low fluctuations thereof, while for the higher Stokes numbers the TKE rises by almost an order of magnitude, and oscillates dramatically over time.

To characterize the fluctuations of the local particle concentration we follow the method of the Voronoï tessellation.[14] In this approach the domain is divided into cells defined based on the particle positions. In Fig. 5 we plot the probability density functions of the volumes of the Voronoï cells v which is a measure of the local particle concentration for the different Stokes numbers, and compare them to the case of particles being spatially distributed as in a Poisson process. For both high and

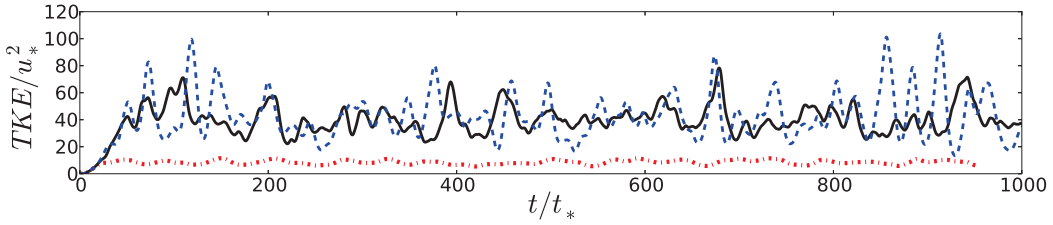

FIG. 4. Time evolution of the turbulent kinetic energy normalized with $u_* = \ell_*/t_*$ for $St = 0.074$ (dotted line, red), 0.35 (plain line, black), and 7.3 (dashed line, blue) for $\gamma = 83$ and $C = 0.35$.

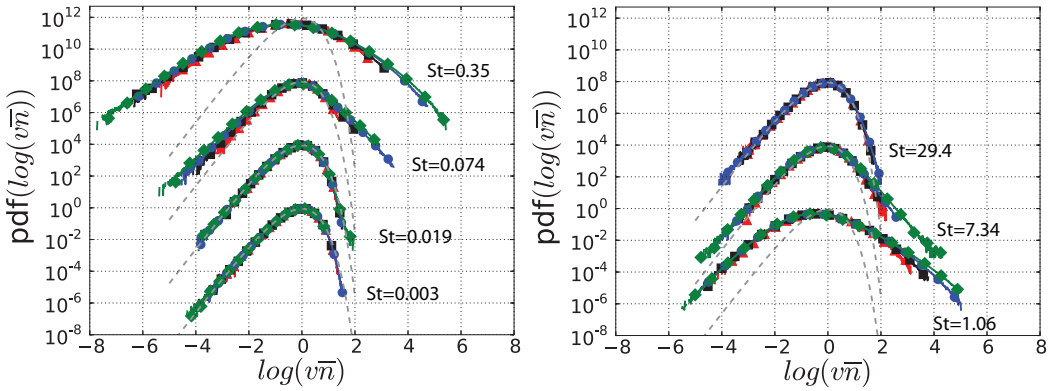

FIG. 5. PDF of the logarithm of the normalized volume of the Voronoï cell, for different Stokes numbers, for $\gamma = 48$ (triangles, red), 83 (squares, black), 190 (circles, blue), and 330 (diamonds, green), and for $C = 0.19$. Each PDF is compared with the PDF (dashed lines) corresponding to the Poisson distribution.

low Stokes number ($St = 0.003$, 0.019, and 29.4), the distributions are close to the Poisson case, i.e., the particles are nearly homogeneously distributed. At intermediate Stokes numbers ($St = 0.074$, 0.35, 1.06, and 7.34), the Voronoï volume distribution becomes much broader, which is the signature of intense particle clustering.

Next, we ask whether the mechanism that leads to the non-uniform distribution of particles with Stokes number of order one is similar to the one acting in classic homogeneous turbulence, where heavy particles tend to be centrifuged out of vortex cores and accumulate in highly strained areas.[15] In Fig. 6(a) the relative fraction of particles in rotating regions (identified by negative values of discriminant of the velocity gradient tensor[16] $\sigma_{ij} = \partial u_i/\partial x_j$: $\Delta = (\det(\sigma)/2)^2 - (\mathrm{Tr}(\sigma)/6)^3 < 0$), is plotted as function of Stokes number. The number of particles in rotating regions is at a minimum for $St = O(1)$, as it is found in simulations of homogeneous isotropic turbulence with forcing at low wave numbers.[17] The coincidence of $St = O(1)$ for maximum segregation is quite remarkable, given that our definition of St is also different from that in the classical homogeneous turbulence. Moreover, the present case is profoundly different, in that the flow itself is driven by particle segregation, and is not given *a priori*. This is illustrated also in Fig. 6(a) where the relative volume of rotation-dominated regions (with $\Delta < 0$) is plotted as a function of Stokes number. It is seen that the fraction of the rotation-dominated volume decreases as St is increased. This is likely to be due to the strain generated by the upward motion of relatively hot plumes. The particles are the source of the buoyancy-induced fluctuations, which are more intense when the clustering is more

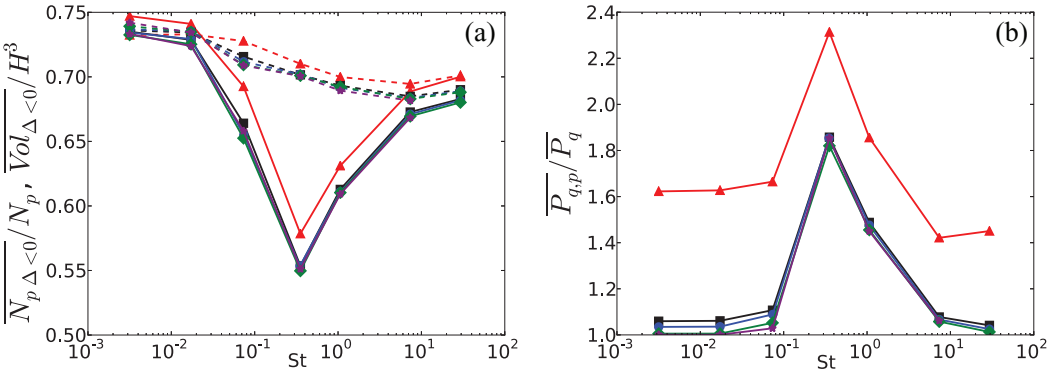

FIG. 6. (a) Effect of Stokes number on the relative number of particles in rotating regions (continuous lines) and mean volume of rotation-dominated region normalized by the domain volume (dashed lines). (b) Mean production of enstrophy at the particle locations normalized by the mean enstrophy production as a function of St. For both figures: $\gamma = 83$ and $C = 0.035$ (triangles, red), 0.19 (squares, black), 0.35 (circles, blue), 1.82 (diamonds, green), 8.77 (stars, purple).

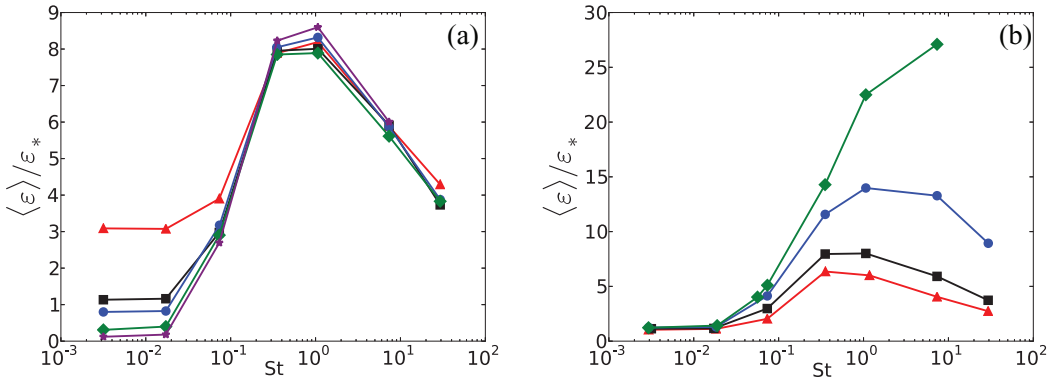

FIG. 7. Evolution with the Stokes number of the mean turbulent kinetic energy dissipation, normalized by ϵ_*. (a) For $C = 0.035$ (triangles, red), 0.19 (squares, black), 0.35 (circles, blue), 1.82 (squares, green), 8.77 (stars, purple) with $\gamma = 83$. (b) For $\gamma = 48$ (triangles, red), 83 (squares, black), 190 (circles, blue), and 330 (diamonds, green) with $C = 0.19$.

pronounced. This is seen in Fig. 6(b), that displays the enstrophy production due to buoyancy,[18] $P_q = \alpha g(\omega_1 \partial\theta/\partial x_2 - \omega_2 \partial\theta/\partial x_1)$, with ω being the vorticity, at the particle locations normalized by the mean enstrophy production of the flow, as a function of the Stokes number. The curves maxima at Stokes numbers of order one confirms that the preferential particle concentration is at the same time cause and consequence of the turbulence generation, in accordance to the feedback mechanism outlined above (Fig. 1).

Finally, we explore the effects of mean particle concentration and domain size. In Fig. 7(a) we present the turbulent dissipation rate (averaged both spatially and temporally for $(t/t_* > 100)$ versus the Stokes number, for five mean particle concentrations and one domain size. Values are normalized by $\epsilon_* = \alpha g \beta \ell_*$. As expected, the dissipation peaks at $St = O(1)$, reflecting the high generation of enstrophy. For $St > 0.074$ the normalized dissipation is negligibly influenced by particle concentration (i.e., all of the dependence is captured in the normalized definition of dissipation), but for the lower Stokes numbers the normalized dissipation increases with decreasing concentration. Fig. 7(b) shows the evolution of the turbulent dissipation with the Stokes number for different domain sizes, keeping constant the mean particle concentration. For small particle inertia the domain size does not play a role, but at higher Stokes numbers the turbulence dissipation increases with γ. Analogous trends are found for the turbulent kinetic energy and the fluid temperature variance. We deduce that, a qualitative change in the scaling behavior occurs with increasing St. For marginal particle inertia (hence weak clustering), the forcing depends on the mean inter-particle distance, which increases with decreasing particles concentration. On the other hand, at higher Stokes numbers, the forcing is related to the clusters size and inter-cluster distance, which fluctuate in a range of scales limited only by the domain size.

We have reported the first study of the interaction between particle-laden flow, thermal radiation, and buoyancy forcing. Buoyancy-driven motions around hot particles produce clusters, causing larger temperature and density fluctuations, and therefore stronger fluid agitation that eventually develops into turbulence. We underline that this phenomenon is fundamentally different from particle-laden turbulent flows forced at large scales, in that here the dispersed phase represents the means through which the energy is injected. In this sense the present regime shares similarities with turbulence in living fluids,[19] and bubble-induced pseudo-turbulence.[20–22] However, unlike in those situations, the present dynamics is self-sustained, i.e., the response of the fluid to the forcing enhances the forcing itself. Because this mechanism stimulates and enhances particle clustering, it is potentially relevant for several phenomena in which concentration-driven coalescence is critical. Equally important, it demonstrates a novel route to turbulence in dispersed multiphase flows subject to radiation.

We gratefully acknowledge fruitful comments by John Eaton on a draft of this letter. R.Z. acknowledges support from Bosch LLC. The support of the Charles Lee Powell Foundation (PI: A.M.) and the France-Stanford Center for Interdisciplinary Studies through a collaborative project grant (PIs: P. Moin / M.M.), is gratefully acknowledged.

[1] S. Balachandar and J. K. Eaton, "Turbulent dispersed multiphase flow," Annu. Rev. Fluid Mech. **42**, 111–133 (2010).
[2] R. Shaw, "Particle-turbulence interactions in atmospheric clouds," Annu. Rev. Fluid Mech. **35**, 183–227 (2003).
[3] J. N. Cuzzi, R. C. Hogan, J. Paque, and A. Dobrovolskis, "Self-selective concentration of chondrules and other small particles in protoplanetary nebula turbulence," Astrophys. J. **546**, 496–508 (2001).
[4] H. Watanabe, R. Kurose, S. Komori, and H. Pitsch, "Effects of radiation on spray flame characteristics and soot formation," Combust. Flame **152**, 2–13 (2008).
[5] F. J. Miller and R. W. Koenigsdorff, "Thermal modeling of a small-particle solar central receiver," J. Sol. Energy Eng. **122**, 23–29 (2000).
[6] F. Doisneau, F. Laurent, A. Murrone, J. Dupays, and M. Massot, "Eulerian multi-fluid models for the simulation of dynamics and coalescence of particles in solid propellant combustion," J. Comput. Phys. **234**, 230–262 (2013).
[7] K. Deshmukh, D. Haworth, and M. Modest, "Direct numerical simulation of turbulence-radiation interactions in homogeneous nonpremixed combustion systems," Proc. Combust. Inst. **31**, 1641–1648 (2007).
[8] K. Matsuda, R. Onishi, R. Kurose, and S. Komori, "Turbulence effect on cloud radiation," Phys. Rev. Lett. **108**, 224502 (2012).
[9] P. J. Coelho, "Numerical simulation of the interaction between turbulence and radiation in reactive flows," Prog. Energy Combust. Sci. **33**, 311–383 (2007).
[10] In a separate analysis we have confirmed that our qualitative conclusions do not change for particles with finite heat capacity, however to enable focus on the key physics we here consider the simple limit of local thermal equilibrium.
[11] V. Väisälä, "Über die wirkung der windschwankungen auf die pilotbeobachtungen," Societas Scientiarum Fennica, Commentationes Physico Mathematicaea II **2**, 38 (1925).
[12] V. Borue and S. A. Orszag, "Turbulent convection driven by a constant temperature gradient," J. Sci. Comput. **12**, 305–351 (1997).
[13] M. Maxey, B. Patel, E. Chang, and L. Wang, "Simulations of dispersed turbulent multiphase flow," Fluid Dyn. Res. **20**, 143–156 (1997).
[14] R. Monchaux, M. Bourgoin, and A. Cartellier, "Preferential concentration of heavy particles: A Voronoi analysis," Phys. Fluids **22**, 103304 (2010).
[15] K. D. Squires and J. K. Eaton, "Preferential concentration of particles by turbulence," Phys. Fluids A **3**, 1169–1178 (1991).
[16] M. S. Chong, A. E. Perry, and B. J. Cantwell, "A general classification of three-dimensional flow fields," Phys. Fluids A **2**, 765–777 (1990).
[17] J. Bec, L. Biferale, G. Boffetta, A. Celani, M. Cencini, A. Lanotte, S. Musacchio, and F. Toschi, "Acceleration statistics of heavy particles in turbulence," J. Fluid Mech. **550**, 349–358 (2006); see http://journals.cambridge.org/article_S002211200500844X.
[18] S. Balachandar, "Structure in turbulent thermal convection," Phys. Fluids A **4**, 2715–2726 (1992).
[19] H. H. Wensink, J. Dunkel, S. Heidenreich, K. Drescher, R. E. Goldstein, H. Löwen, and J. M. Yeomans, "Meso-scale turbulence in living fluids," Proc. Natl. Acad. Sci. U.S.A. **109**, 14308–14313 (2012).
[20] M. Lance and J. Bataille, "Turbulence in the liquid phase of a uniform bubbly air–water flow," J. Fluid Mech. **222**, 95–118 (1991).
[21] J. Martínez Mercado, D. Chehata Gomez, D. Van Gils, C. Sun, and D. Lohse, "On bubble clustering and energy spectra in pseudo-turbulence," J. Fluid Mech. **650**, 287–306 (2010).
[22] G. Riboux, D. Legendre, and F. Risso, "A model of bubble-induced turbulence based on large-scale wake interactions," J. Fluid Mech. **719**, 362–387 (2013).